# Crystal Structures, Optical Properties, and Effective Mass Tensors of CH3NH3PbX3 (X = I and Br) Phases Predicted from HSE06 (vol 5, pg 1278, 2014)

**ARTICLE** *in* JOURNAL OF PHYSICAL CHEMISTRY LETTERS · MARCH 2014

Impact Factor: 7.46 · DOI: 10.1021/jz500480m



**2 AUTHORS:**

Jing Feng
Wuhan University
**249** PUBLICATIONS **3,624** CITATIONS
SEE PROFILE

Bing Xiao
University College London
**76** PUBLICATIONS **992** CITATIONS
SEE PROFILE

THE JOURNAL OF PHYSICAL CHEMISTRY Letters

Letter

pubs.acs.org/JPCL

# Crystal Structures, Optical Properties, and Effective Mass Tensors of $CH_3NH_3PbX_3$ (X = I and Br) Phases Predicted from HSE06

Jing Feng[†] and Bing Xiao*[,‡,§]

[†]School of Engineering and Applied Science, Harvard University, Cambridge, Massachusetts 02138, United States

[‡]Department of Physics, College of Science and Engineering, Temple University, Philadelphia, Pennsylvania 19122, United States

Supporting Information

**ABSTRACT:** The crystal structures are successfully established for tetragonal and orthorhombic $CH_3NH_3PbX_3$ (X = I and Br). The equilibrium lattice parameters are computed by the DFT+D2 method, and the results are compared to experimental values. The band dispersions and electronic densities of states are calculated by HSE06, showing that their band gaps are in the range from 1.63 to 2.3 eV. Although the calculated dielectric functions of $MAPbX_3$ compounds are similar to other semiconductors, the absorption spectra of their bulk crystals are drifted away from visible light spectrum. The effective mass tensors of holes and electrons are also evaluated in three principal directions at the Γ point. The anisotropies in the effective masses of the hole and electron are illustrated for two orthorhombic phases.

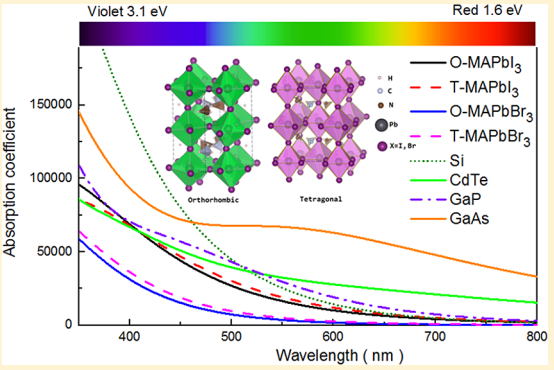


**SECTION:** Energy Conversion and Storage; Energy and Charge Transport

Photovoltaics (PVs) are considered as an ideal energy conversion process.[1,2] Solar cells based on semiconductors exhibit power conversion efficiencies (PCEs) of about 12−25%.[3] Recently, methylammounium (MA) triiodideplumbate and its derivatives ($CH_3NH_3PbX_3$, X = I, Br, Cl) attracted much attention because of their lower manufacturing costs and high performance in conversion of solar light into electrical power (PCEs exceeding 15%).[4,5] Snaith[6] et al. and Xing and Gratzel[7] independently reported the diffusion length measurements performed on hybrid perovskites, which showed that the effective diffusion lengths are indeed relatively large in $CH_3NH_3PbI_3$ films, about 100 nm for both electrons and holes, a high value for a semiconductor formed from solution at low temperature. The highly efficient solar cell should be able to absorb over a wide range of spectra, from visible to near-infrared wavelengths (320−1000 nm), converting the incident photon energy effectively into movable charges. Hence, the electronic structure of a solar energy harvester should have a suitable optical band gap, enabling absorption of different photons in the solar spectrum.[8] Moreover, the high mobility of carriers is important, because it requires that the light-generated electrons and holes can move large enough distances to be extracted as current, instead of losing their energy as heat within the cell.[9,10] Kawamura[11] and Poglitsch[12] have determined the crystal structures of $MAPbX_3$ pervoskites; however, the coordinates of hydrogen atoms in their structures were not obtained by X-ray diffraction. As Loi and Hummelen[1] said, "what is the mobility of electrons and holes? What is the exact atomic structure of the hybrid perovskites and how do different structures influence the transport properties of the photoexcitations?" We still do not know the exact crystal structures of $MAPbX_3$ pervoskites. Here, we reconstructed the exact crystal structures of tetragonal (T)- and orthorhombic (O)-$MAPbX_3$ phases from the existing crystallographic data and group theory. By applying the first-principles calculations, we discussed the electronic structures and optical properties of those crystals. We also calculated the effective mass tensors of electrons and holes of $MAPbX_3$ pervoskites, and the anisotropies in effective masses of carriers have been addressed in this Letter.

The details and methods used in this Letter are in the Supporting Information. From the previous experiments and theoretical studies, it is known that the fundamental building blocks in $CH_3NH_3PbX_3$ structures are the organic $(CH_3NH_3)^+$ cation and $(PbX_3)^-$ framework. The latter inorganic anion forms the $PbX_6$ octahedral in the crystal structure of $CH_3NH_3PbX_3$, which is completely analogous to the pervoskite-type structure. The atomic positions of anions in either the T- or O-$MAPbX_3$ (MA represents $CH_3NH_3$) phase are rigid and in the ordered state. Using the conventional single-crystal X-ray diffraction method, Barkie[13] et al. and Kawamura[11] et al. reported the exact coordinates of $PbX_3$ anions in the O and T phases of $MAPbI_3$, respectively. In addition, for the O-$MAPbI_3$, the $(CH_3NH_3)^+$ cations are also ordered in the crystal structure. The atomic positions of N and C were also determined by Barkie and co-workers.[13] Because

**Received:** March 6, 2014
**Accepted:** March 24, 2014

   dx.doi.org/10.1021/jz500480m | J. Phys. Chem. Lett. 2014, 5, 1278−1282

the H atoms in the crystal structure are almost transparent to the X-ray diffraction, the coordinates of all H atoms were not given in ref 13. On the other hand, the $(CH_3NH_3)^+$ cations in T-$MAPBI_3$ are completely in a disordered state. Although the atomic positions of N and C have been measured in ref 11, the fractional occupancies of the two elements in the crystal structure have serious difficulty studying the electronic and optical properties using the routine density functional theory (DFT) method. In this Letter, the crystal structure of O-$MAPbI_3$ was built using the data in ref 13 except for the coordinates of H atoms. For H atoms in O-$MAPbI_3$, we have reconstructed their positions from the point groups and multiplicities of Wyckoff sites under the space group *Pnam* (see the Supporting Information for the details). In the case of T-$MAPbI_3$, it has been shown that there are three equivalent configurations for disordered $(CH_3NH_3)^+$ cations in the crystal structure. In our work, the $(CH_3NH_3)^+$ cations are aligned in eight possible ⟨111⟩ directions, which correspond to the Model (C) in ref 11. Because $(CH_3NH_3)^+$ cations are completely disordered, we only require the main rotating axis of each $CH_3NH_3$ unit be pointed to one of eight ⟨111⟩ directions. For the cation itself, C and N atoms are allowed to switch their positions freely. As a result, in our current model of the T-$MAPbI_3$ structure, the four $(H_3C{-}NH_3)^+$ cations aligned in ⟨111⟩ directions actually have two different types, that is, half of them are arranged as $(H_3C{-}NH_3)^+$ and the remaining two are configured as $(H_3N{-}CH_3)^+$. The coordinates of H atoms in the T-phase were derived in the same way as those of the O-phase. Due to the structural disorder, the actual space group of T-$MAPbX_3$ (X = I and Br) structures is *P*1 in our calculations. Finally, the crystal structures of T- and O-phases of $MAPbBr_3$ were obtained by substituting the iodine with bromine in the corresponding phases of $MAPbI_3$. The crystal structures of both T- and O-phases of $MAPbX_3$ are illustrated in Figure 1.

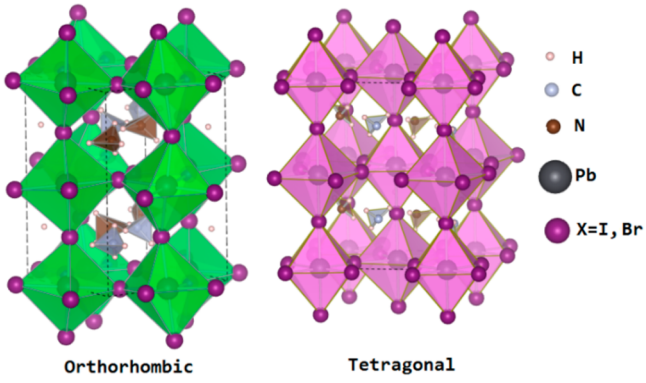


**Figure 1.** The crystal structures of T- and O-$CH_3NH_3PbX_3$ (X = I and Br) phases. The rigid framework consisting of the $PbX_6$ octahedral is also highlighted in the structure.

Wang[14] et al. showed that the van der Waals interactions are important in $MAPbX_3$ crystal structures. The good lattice constants can only be obtained using the DFT method within van der Waals corrections. In this work, the dispersion interactions were computed from an empirical pairwise corrections proposed by Grimme[15] in terms of the DFT+D2 scheme, and the calculated values were compared with experimental results, as shown in Table s1 (Supporting Information). We show that the optimized structural parameters of T- and O-$CH_3NH_3PbX_3$ (X = I and Br) phases are in excellent agreement with experiments, implying the intrinsic flaw of applying the empirical pairwise corrections[14] in the structural predictions for van der Waals bound solids. The detailed discussions are in the Supporting Information. The electronic structures of T- and O-phases of $MAPbX_3$ were calculated using HSE06[16] in this work because the hybrid density functional usually gives the accurate fundamental band gaps for most semiconductors. The results are illustrated in Figure s2 in the Supporting Information. From the results of band gaps, we can see that all $MAPbX_3$ compounds are not colorless and transparent to the visible light spectrum. This conjecture has been confirmed experimentally.[17] For example, the single crystal of $MAPbI_3$ synthesized by Barkie[13] et al. is black, and the $MAPbBr_3$ nanoparticles dispersed in the organic solvents show colors from light green to yellow.[18] Otherwise, due to the smaller band gaps of $MAPbX_3$ compounds, they might be useful in harvesting the solar energy at a particular wavelength. We would like to compare the computed band gaps of T- and O-$MAPbX_3$ (X = I and Br) to those experimental values. Clearly, HSE06 gives the best results for all structures.

The densities of states of T- and O-$MAPbX_3$ structures are shown in Figure s2 (Supporting Information). The chemical interactions and bonding mechanisms of them have been discussed in the Supporting Information.[14,19−23] The main interaction between the $(MA)^+$ cation and $(PbX_3)^-$ is ionic. The electronic states of the $(NH_3CH_3)^+$ cation are separated from the main part of the valence band near the Fermi level, and their single-particle energies are also lower than most electronic states of the $(PbX_3)^-$ anion. Our results are consistent with the previous publications, that is, O-$MAPbI_3$,[14] cubic- and O-$MAPbI_3$,[19,20] and pseudocubic-$MAPbI_3$.[23] Otherwise, the bonding mechanism of the $(MA)^+$ cation is mainly covalent bonds. The $\sigma$- and $\pi$-bonds are formed from the 2p states of C and N atoms. In addition, the strong mixing of H 1s states with those 2p states of either the N or C atom indicates the strong covalent nature of H−C and H−N bonds. The chemical bonds in the $PbX_6$ octahedral are also found to be polar-covalent. Our work indeed reveals results similar to those of Umebayshi[20] et al. for the valence band, which explained that the top of the valence band of cubic- or O-$MAPbI_3$ mainly consists of $\sigma$-antibonding states of Pb 6s and I 5p while the bottom of the conduction band is attributed to $\sigma$-antibonding states of Pb 6p and I 5s. For the bottom of the conduction band, we find that the 6p states of Pb play the central role. Because both the valence and conduction bands are dominated by p states, the photon-induced direct transition probability might be low due to the selection rule.

In order to study the solar energy harvesting property of T- and O-$MAPbX_3$ (X = I and Br) structures, we have calculated the dielectric function and absorption spectrum for each of them. For the computed details, we refer the readers to ref 24. The imaginary and real parts of the dielectric function are displayed in Figure 2. For the computed structures, their dielectric spectra in the imaginary part show two peaks below 400 nm. Above this wavelength, the imaginary parts of them go down to zero. We should note that the computed intensities of the imaginary part for T- and O-$MAPbI_3$ are higher than those of $MAPbBr_3$ phases. The main reason is that the fundamental band gaps of the latter phases are larger than the former structures. As a result, the transition probability is reduced in the $MAPbBr_3$ case according to the Fermi-Golden rule. Due to the strong absorption near 160 nm, the real parts of the


dx.doi.org/10.1021/jz500480m | *J. Phys. Chem. Lett.* 2014, 5, 1278−1282

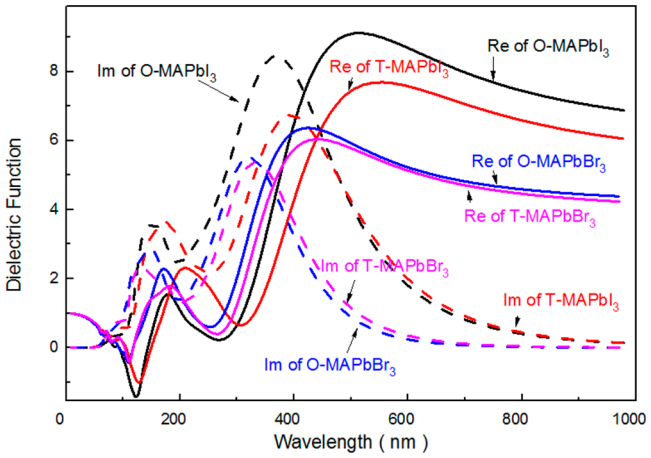


**Figure 2.** The dielectric spectra of T- and O-$MAPbX_3$ (X = I and Br) structures.

dielectric spectrum of T- and O-$MAPbX_3$ structures became negative. Thus, their crystals are completely not transparent to the ultraviolet spectrum around that wavelength. The second prominent absorption is seen near 300 nm in the computed dielectric spectra of T- and O-$MAPbX_3$ structures. This wavelength is basically located at the near-ultraviolet spectrum. So far, from the computed dielectric spectra of $MAPbX_3$ compounds, it is unlikely that their bulk crystals can be considered as good solar energy absorbers in the visible light spectrum. In order to verify this conclusion, we show the calculated absorption spectra of $MAPbX_3$ (X = I and Br) structures in Figure 3, including, Si, CdTe, GaP, and GaAs. It is

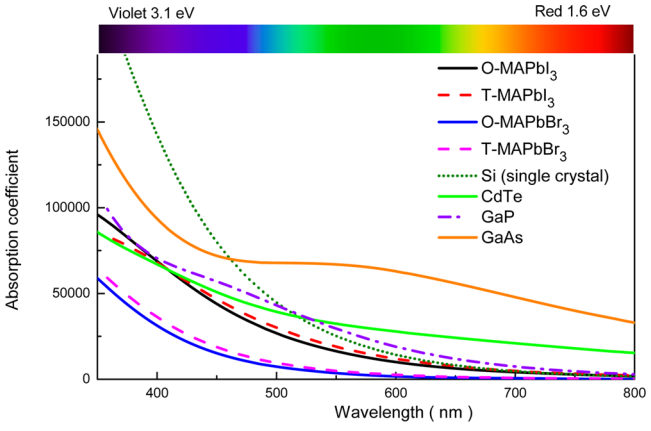


**Figure 3.** The comparison of the absorption spectra of T- and O-$MAPbX_3$ (X = I and Br) structures with those of Si, CdTe, GaP, and GaAs in the visible light spectrum.

now clear that the overall solar energy absorption efficiencies of bulk T- and O-$MAPbX_3$ phases in the entire visible light spectrum are not superior to any of the other four widely used semiconductors in solar cells. GaAs shows strong absorption in the full solar spectrum. Si is better than other materials in the near-edge of the visible light spectrum. The T- and O-$MAPbX_3$ only respond strongly to the ultraviolet spectrum. Because the strongest output of solar energy is attributed to visible light spanning in a narrow range between 380 to 780 nm (44%), the total power output of visible light plus the infrared spectrum consists of 92% of total solar energy.

The effective mass of the hole or electron at the band extremes is related to the band dispersion as

$$E(\vec{k}) = E(\vec{k}_0) \pm \frac{\hbar^2}{2}[\vec{k}_i - \vec{k}_0][S_{ij}][\vec{k}_j - \vec{k}_0]^T \quad (1)$$

where $E(\vec{k}_0)$ represents the eigenenergies at the band extremes, that is, the values at the $\vec{k}_0$ in the Brillouin zone. The tensor $S_{ij}$ is related to the effective mass tensor $m_{ij}^*$ by

$$S_{ij} = \sum_{i=1}^{3}\sum_{i=1}^{3}\frac{1}{m_{ij}^*} \quad (2)$$

where the total effective mass $M^*$ can be computed from $M^* = 1/S_{ij}$. For T- and O-$MAPbX_3$ (X = I and Br) structures, the band extremes are located at the Γ point, Thus, $\vec{k}_0 = 0$. Due to the symmetry of the crystal structure, the effective mass tensors of T- and O-$MAPbX_3$ (X = I and Br) have the following forms

$$S_{ij}(\text{Tetragonal}) = \begin{pmatrix} S_{11} & 0 & 0 \\ 0 & S_{11} & 0 \\ 0 & 0 & S_{33} \end{pmatrix} \quad (3)$$

$$S_{ij}(\text{Orthorhombic}) = \begin{pmatrix} S_{11} & 0 & 0 \\ 0 & S_{22} & 0 \\ 0 & 0 & S_{33} \end{pmatrix} \quad (4)$$

In the matrices (eqs 3 and 4), the $S_{11}$, $S_{22}$, and $S_{33}$ refer to the inverses of effective masses of either the hole or electron in the [100], [010], and [001] directions. By fitting the obtained band dispersions in these three principal directions near the Γ point within eq 1, we have computed the effective masses of holes and electrons for T- and O-$MAPbX_3$ (X = I and Br) phases, as shown in Table s2 (Supporting Information). The values of them are typical for semiconductors except the O-$MAPbI_3$. The hole effective mass of O-$MAPbI_3$ in the [010] direction is 11.979 $m_e$, which is the largest value among all studied $MAPbX_3$ (X = I and Br) structures. Otherwise, if we compare the computed effective masses of T- and O-$MAPbX_3$ structures to Si ($m_e^*$ = 0.19 $m_e$ at the Δ point and the light hole at 0.19 $m_e$ and heavy hole at 0.53 $m_e$ at the Γ point), we can see that the latter material is still better than the former ones. Giorgi et al.[23] computed the effective masses of the hole and electron for pseudocubic-$MAPbI_3$; their effective mass of the hole without including the spin−orbital coupling is 0.36 $m_e$. We find that the number is identical to our value for the T-$MAPbI_3$ in the [001] direction. One should note that the [001] direction in cubic-$MAPbI_3$ is equivalent to the same direction in the T-phase.

The effective mass of either the hole or electron in an arbitrary direction infinitesimally close to the Γ point can be obtained using the following relationship

$$S_{11} = \sum_{m=1}^{3}\sum_{n=1}^{3}\lambda_{1m}\lambda_{1n}S_{mn} \quad (5)$$

In the equation, $\lambda_{1m}$ refers to the directional cosines with respect to three principal directions. For T and O crystal classes, eq 5 can be simplified as

$$M^* = \frac{1}{\cos^2(\alpha)S_{11} + \cos^2(\beta)S_{22} + \cos^2(\gamma)S_{33}} \quad (6)$$


dx.doi.org/10.1021/jz500480m | J. Phys. Chem. Lett. 2014, 5, 1278−1282

where $\alpha$, $\beta$, and $\gamma$ are the angles between that specific direction and the [100], [010], and [001] directions, respectively. For T-$MAPbX_3$ (X = I and Br) phases, we have $S_{11} = S_{22}$ in eq 3. Here, we plot the three-dimensional contours of effective masses of holes and electrons for two O-$MAPbX_3$ structures. The results are illustrated in Figure 4. The effective mass of the hole in the O-$MAPbI_3$ phase shows the strongest anisotropic contour, as implied in Figure 4b, due to its unusual heavy hole mass in the [010] direction.

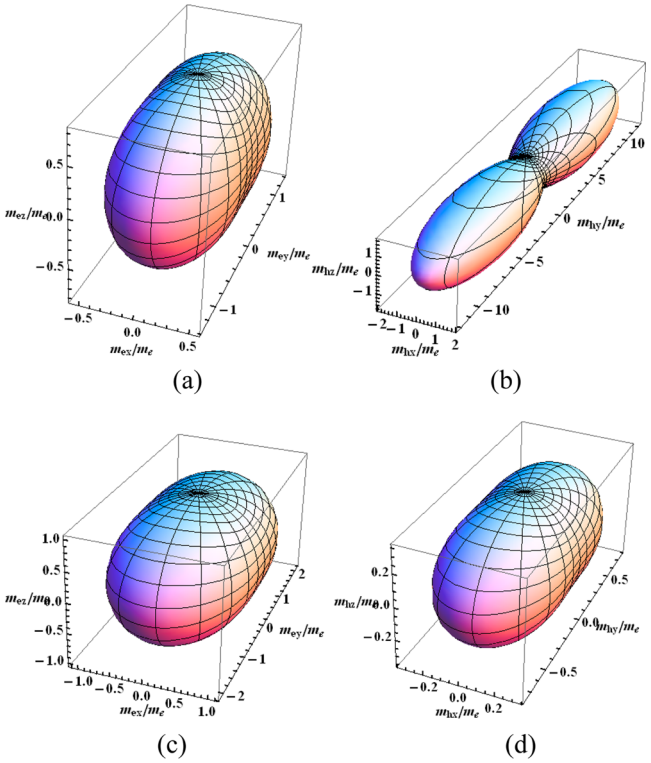


**Figure 4.** The three-dimensional contour plots of the effective masses of holes and electrons in an arbitrary direction infinitesimally close to the Γ point for O-$MAPbX_3$ (X = I and Br). (a) $m_e^*$ of O-$MAPbI_3$; (b) $m_h^*$ of O-$MAPbI_3$; (c) $m_e^*$ of O-$MAPbBr_3$; (d) $m_h^*$ of O-$MAPbBr_3$.

In summary, we have employed DFT+D2 and HSE06 to study the equilibrium lattice parameters, electronic structures, and optical properties of T- and O-$MAPbX_3$ (X = I and Br) phases. We found that van der Waals interactions are important for obtaining the accurate equilibrium cell volumes from DFT. From the computed band structures and electronic densities of states, we concluded that all computed structures are semiconductors with direct band gaps at the Γ point using HSE06. From the computed effective mass tensors for holes and electrons, both T- and O-$MAPbI_3$ phases are also not superior to several widely used semiconductors (Si and GaAs) in solar cells. Thus, T- and O-$MAPbX_3$ (X = I and Br) are considered as trivial semiconductors in their bulk states.

## ■ ASSOCIATED CONTENT

### Supporting Information

Details and the method of $MAPbX_3$ compounds used in this work. This material is available free of charge via the Internet at http://pubs.acs.org.

## ■ AUTHOR INFORMATION


### Corresponding Author

*E-mail: bingxiao@temple.edu. Tel: +1-215-900-4820.

### Present Address

§B.X.: Barton Hall A205, Department of Physics, College of Science and Engineering, Temple University, Philadelphia, PA 19122, U.S.A.


### Author Contributions

Jing Feng provided the idea and calculated the properties, and Bing Xiao participated in the discussion and wrote the main part of the paper.

### Notes

The authors declare no competing financial interest.

## ■ ACKNOWLEDGMENTS

Research financed by the National Scholarship Council under Grant No. 201208530028.

## ■ REFERENCES


(1) Loi, M. A.; Hummelen, J. C. Hybrid Solar Cells: Perovskites under the Sun. *Nat. Mater.* **2013**, *12*, 1087−1089.

(2) Kazim, S.; Nazeeruddin, Md. K.; Grätzel, M.; Ahmad, S. Perovskite As Light Harvester: A Game Changer in Photovoltaics. *Angew. Chem., Int. Ed.* **2014**, *53*, 2−15.

(3) Kojima, A.; Teshima, K.; Shirai, Y.; Miyasaka, T. Organometal Halide Perovskites As Visible-Light Sensitizers for Photovoltaic Cells. *J. Am. Chem. Soc.* **2009**, *131*, 6050−6051.

(4) Burschka, J.; Pellet, N.; Moon, S.; Humphry-Baker, R.; Gao, P.; Nazeeruddin, Md. K.; Grätzel, M. Sequential Deposition As a Route to High-Performance Perovskite-Sensitized Solar Cells. *Nature* **2013**, *499*, 316−319.

(5) Liu, M.; Johnston, M. B.; Snaith, H. J. Efficient Planar Heterojunction Perovskite Solar Cells by Vapour Deposition. *Nature* **2013**, *501*, 395−398.

(6) Stranks, S. D.; Eperon, G. E.; Grancini, G.; Menelaou, C.; Alcocer, J. P.; Leijtens, T.; Herz, L. M.; Petrozza, A.; Snaith, H. J. Electron−Hole Diffusion Lengths Exceeding 1 Micrometer in an Organometal Trihalide Perovskite Absorbe. *Science* **2013**, *342*, 341−344.

(7) Xing, G.; Mathews, N.; Sun, S.; Lim, S. S.; Lam, Y. M.; Gratzel, M.; Mhaisalkar, S.; Sum, T. C. Long-Range Balanced Electron- and Hole-Transport Lengths in Organic−Inorganic $CH_3NH_3PbI_3$. *Science* **2013**, *342*, 344−347.

(8) Lee, M. M.; Teuscher, J.; Miyasaka, T.; Murakami, T. N.; Snaith, H. J. Efficient Hybrid Solar Cells Based on Meso-Superstructured Organometal Halide Perovskites. *Science* **2012**, *338*, 643−647.

(9) Hodes, G. Perovskite-Based Solar Cells. *Science* **2013**, *342*, 317−318.

(10) Chen, Q.; Zhou, H.; Hong, Z.; Luo, S.; Duan, H.; Wang, H.; Liu, Y.; Li, G.; Yang, Y. Planar Heterojunction Perovskite Solar Cells via Vapor-Assisted Solution Process. *J. Am. Chem. Soc.* **2013**, *136*, 622−625.

(11) Kawamura, Y.; Mashiyama, H.; Hasebe, K. Structural Study on Cubic-Tetragonal Transition of $CH_3NH_3PbI_3$. *J. Phys. Soc. Jpn.* **2002**, *71*, 1694−1697.

(12) POGLITSCH, A.; WEBER, D. Dynamic Disorder in Methylammoniumtrihalogenoplumbates(II) Observed by Millimeter-Wave Spectroscopy. *J. Chem. Phys.* **1987**, *87*, 6373−6378.

(13) Baikie, T.; Fang, Y. N.; Kadro, J. M.; Schreyer, M.; Wei, F. X.; Mhaisalkar, S. G.; Graetzel, M.; White, T. J. Synthesis and Crystal Chemistry of the Hybrid Perovskite $(CH_3NH_3)$ $PbI_3$ for Solid-State Sensitised Solar Cell Applications. *J. Mater. Chem. A* **2013**, *1*, 5628−5641.

(14) Wang, Y.; Gould, T.; Dobson, J. F.; Zhang, H.; Yang, H.; Yao, X.; Zhao, H. Density Functional Theory Analysis of Structural and

Electronic Properties of Orthorhombic Perovskite $CH_3NH_3PbI_3$. *Phys. Chem. Chem. Phys.* **2014**, *16*, 1424−1429.
(15) Grimme, S. Semiempirical GGA-Type Density Functional Constructed with a Long-Range Dispersion Correction. *J. Comput. Chem.* **2006**, *27*, 1787−1799.
(16) Heyd, J.; Scuseria, G. E.; Ernzerhof, M. Hybrid Functionals Based on a Screened Coulomb Potential. *J. Chem. Phys.* **2003**, *118*, 8207−8215.
(17) Maalej, A.; Abid, Y.; Kallel, A.; Daoud, A.; Lautie, A.; Romain, F. Phase Transitions and Crystal Dynamics in the Cubic Perovskite $CH_3NH_3PbCl_3$. *Solid State Commun.* **1997**, *103*, 279−284.
(18) Schmidt, L. C.; Pertegás, A.; González-Carrero, S.; Malinkiewicz, O.; Agouram, S.; Mínguez Espallargas, G.; Bolink, H. J.; Galian, R. E.; Pérez-Prieto, J. Nontemplate Synthesis of $CH_3NH_3PbBr_3$ Perovskite Nanoparticles. *J. Am. Chem. Soc.* **2014**, *136*, 850−853.
(19) Mosconi, E.; Amat, A.; Nazeeruddin, Md. K.; Gratzel, M.; De Angelis, F. First-Principles Modeling of Mixed Halide Organometal Perovskites for Photovoltaic Applications. *J. Phys. Chem. C* **2013**, *117*, 13902−13913.
(20) Umebayashi, T.; Asai, K.; Kondo, T.; Nakao, A. Electronic Structures of Lead Iodide Based Low-Dimensional Crystals. *Phys. Rev. B* **2003**, *67*, 15540515.
(21) Borriello, I.; Cantele, G.; Ninno, D. Ab Initio Investigation of Hybrid Organic−Inorganic Perovskites Based on Tin Halides. *Phys. Rev. B* **2008**, *77*, 23521423.
(22) Chiarella, F.; Zappettini, A.; Licci, F.; Borriello, I.; Cantele, G.; Ninno, D.; Cassinese, A.; Vaglio, R. Combined Experimental and Theoretical Investigation of Optical, Structural, And Electronic Properties of $CH_3NH_3SnX_3$ Thin Films (X=Cl,Br). *Phys. Rev. B* **2008**, *77*, 0451294.
(23) Giorgi, G.; Fujisawa, J.; Segawa, H.; Yamashita, K. Small Photocarrier Effective Masses Featuring Ambipolar Transport in Methylammonium Lead Iodide Perovskite: A Density Functional Analysis. *J. Phys. Chem. Lett.* **2013**, *4*, 4213−4216.
(24) Feng, J.; Xiao, B.; Pan, W.; Jiang, Y. H.; Zhou, R. $LiRE_2Si_3$ (RE = Nd, Sm, and Eu) As Potential Photovoltaic Materials. *Appl. Phys. Lett.* **2013**, *103*, 013902.